

Evaluation of the redox performance and characterization of Fe₂O₃/CeO₂/ZrO₂ oxygen carriers at high temperature in-situ gasification chemical-looping combustion (iG-CLC) conditions

*Nicholas C. Means ^{*a,c}, Sonia Hammache ^{a,c}, Ward A. Burgess ^{a,c}, Bret H. Howard ^a, Mark W. Smith ^b*

^a National Energy Technology Laboratory, 626 Cochrans Mill Road, P.O. Box 10940, Pittsburgh, PA 15236-0940, USA

^b National Energy Technology Laboratory, 3610 Collins Ferry Road, Morgantown, WV 26507, USA

^c Leidos Research Support Team, 626 Cochrans Mill Road, P.O. Box 10940, Pittsburgh, PA 15236-0940, USA

*Corresponding Author: E-mail: Nicholas.Means@NETL.DOE.GOV; Tel: 1-412-386-5847

Keywords: chemical-looping combustion; in-situ gasification; oxygen carrier; iron oxide; ceria; zirconia; drop tube reactor

Abstract

Iron-based oxygen carriers with CeO₂ support have interesting redox applications in chemical-looping combustion (CLC). CeO₂ behaves as an active support for many oxygen carrier applications due to the reversible release of lattice oxygen. High temperature processes may lead to improved process efficiency, however the poor thermal stability of CeO₂ gives rise to a need for oxygen carriers that can resist sintering and agglomeration and maintain reactivity after multiple reduction and oxidation (redox) cycles during in-situ gasification chemical-looping combustion (iG-CLC) at 1100°C. In the present study, Fe-based oxygen carriers on CeO₂, ZrO₂ and Ce_{0.75}Zr_{0.25}O₂ supports were prepared by a co-precipitation method. The redox stability, reactivity and sintering of the oxygen carriers were evaluated to investigate the effect of the CeO₂-ZrO₂ solid solution support. The oxygen transport capability was evaluated in a drop tube fixed bed reactor under iG-CLC conditions with coal char at 1100°C for 10 redox cycles. The CeO₂-ZrO₂ solid solution improved the oxygen mobility of the support from the creation of more oxygen defects. The Fe-Ce oxygen carrier had the highest oxygen transport capability due to the formation of cerium orthoferrite (CeFeO₃) during high temperature reduction. The Fe-Ce-Zr oxygen carrier showed improved reactivity over the Fe-Ce oxygen carrier as the number of redox cycles increased. The oxygen carriers, before and after multiple redox cycles, were characterized by X-ray diffraction, scanning electron microscopy, and surface/pore analysis.

1. Introduction

The emission of carbon dioxide from power generation poses a significant challenge to the development of clean energy technologies. The need for clean energy cannot yet be entirely met by renewable energy sources alone so technologies using coal are important. Although renewable energy technologies are improving, approximately 36% of the global net electricity generation is expected to

come from coal by 2040 [1]. Carbon capture and storage (CCS) is an enticing process that may be used to reduced CO₂ concentrations in the atmosphere. Capturing CO₂ from a process gas stream is typically a problematic and energy intensive task because of the need to separate CO₂ from N₂ in air [2].

Chemical-looping combustion (CLC) is an attractive technology to generate power and produce a high purity CO₂ stream from the combustion of a fuel material. CLC is a cyclic reaction process that employs an oxygen carrier (OC) material to transfer oxygen from the air to the fuel by oxidation and reduction reactions. This process typically takes place in two connected fluidized bed reactors. Chemical-looping combustion using solid fuel (coal) may be done by in-situ gasification chemical-looping combustion (iG-CLC) where the solid fuel is gasified to produce syngas (CO and H₂). The syngas is then combusted by the oxygen carrier in the fuel reactor. The oxygen carrier is reduced as it combusts the syngas components and then cycled to the air reactor where it is re-oxidized. This cycling is continuous and makes up the iG-CLC process.

Iron-based oxygen carriers are commonly investigated because they are relatively cheap and readily available. Additionally, most Fe-based oxygen carriers have a low environmental impact because they are not toxic [3]. Iron-based oxygen carriers may have many different oxidization states as Fe₂O₃ is reduced to Fe₃O₄, FeO, or Fe. Due to thermodynamic limitations, the reaction (Fe₂O₃ → Fe₃O₄) is ideal for complete combustion of syngas because (Fe₃O₄ → FeO) and (FeO → Fe) will produce CO₂ with equilibrium concentrations of CO and H₂ [4]. Because the goal of chemical-looping combustion is to produce a high purity CO₂ stream, incomplete combustion of the syngas is undesirable. Iron-based oxygen carriers typically have good reactivity with CH₄ and syngas (CO and H₂) and have previously been investigated under various conditions [5-8].

Particle sintering and agglomeration have been shown to occur for Fe-based oxygen carriers during the phase change from FeO to Fe₃O₄ during oxidation [9]. When the oxygen carrier particles sinter

at high temperature, this often leads to agglomeration and poor particle mobility in the bed. This is critical for chemical-looping combustion where the oxygen carrier particles are cycled between the fuel reactor and the air reactor. If particle sintering and agglomeration occurs, the used oxygen carrier will need to be removed from the reactor and replaced with fresh oxygen carrier material. Depending on the severity, this could even cause the reactor to shut down. To avoid significant sintering and maintain CLC reactivity, the iron is commonly supported on various materials such as Al_2O_3 [10, 11], MgO [10], TiO_2 [10, 11] and yttria-stabilized zirconia (YSZ) [11-13]. Recently, oxygen carriers that can withstand high temperatures (1100°C) have been of interest because of the potential benefits of high temperature CLC. Operation of the fuel reactor above 1000°C can reduce required vessel height and eliminate the need for an unconverted char/OC separation unit. As a result, the oxygen carriers need to resist sintering and agglomeration and maintain reactivity after multiple reduction and oxidation cycles at high temperatures.

A loss of reactivity may come from oxygen carrier particle changes during redox cycles resulting in lower porosity and available surface area. The reacting gases CO and H_2 (during reduction) or O_2 (during oxidation) need to be able to access the active sites of the oxygen carrier (iron oxide). Lower oxygen carrier reactivity is often attributed to particle sintering and agglomeration. At high temperatures, sintering of oxygen carrier material occurs where the particles fuse together, and the surface characteristics change. This may affect the oxygen carrier's ability to reduce or oxidize during chemical looping. Reactivity changes due to sintering are of particular interest for high temperature iG-CLC where the fuel reactor would operate at 1100°C . This has been shown to affect iron oxide materials where the pore volume decreases as the reducing temperature increases [14]. Additionally, iron may react with some support materials during reactions at high temperatures, which result in loss of reactivity after multiple redox cycles. Two examples of this are the formation of iron aluminate (FeAl_2O_4) [6] and iron silicate (Fe_2SiO_4) [15]. Although some of the oxygen carrier-support interactions may have a positive

impact on the oxygen transport capability, they create compounds which do not regenerate under multiple redox cycles.

An interesting support for high temperature CLC is ceria (CeO_2). Ceria is often used as a catalyst material support for redox processes such as automotive exhaust conversion [16], removal of SO_x from fluid catalytic cracking (fcc) flue gas [17], catalytic methane oxidation [18, 19] and water gas shift [20]. CeO_2 is a rare-earth metal oxide that has a cubic fluorite structure and can provide/gain oxygen through redox reactions involving $\text{Ce}^{3+} - \text{Ce}^{4+}$ changes. Under oxidizing conditions Ce^{4+} will form CeO_2 and under reducing conditions Ce^{3+} will form Ce_2O_3 [21]. The transformation from Ce^{4+} to Ce^{3+} is associated with a reversible release of lattice oxygen. As a result, CeO_2 has been investigated as an active support for many oxygen carrier applications [22-25]. Oxygen carriers supported with CeO_2 may improve the redox stability of the metal oxide and increase oxygen carrier conversion compared to other support materials [26]. Additionally, CeO_2 -supported Fe-based oxygen carriers were shown to have good reactivity and redox stability at a Fe_2O_3 loading of 60wt% [27]. In a reactivity study at 900°C under CH_4 (reduction), Galinsky et al. [25] showed that iron oxide on CeO_2 had high initial activity but deactivated upon multiple redox cycles. Deactivation was found to occur due to iron migration to the oxygen carrier surface where agglomeration then occurred. This would likely be an even greater problem at higher temperatures and needs to be addressed for high temperature oxygen carriers.

The addition of zirconia (ZrO_2) into CeO_2 forms a solid solution that is known to improve the mechanical and redox properties and thermal stability of the oxygen carrier [28]. The doping of CeO_2 with Zr^{4+} reduces strain within the metal oxide and makes it easier for oxygen defects to form, improving the oxygen mobility. This strain relaxation occurs due to the size difference between the Zr^{4+} and Ce^{4+} cations [27]. Zr^{4+} (84 pm) is smaller than Ce^{4+} (97 pm) [29]. Additionally, Zr doping may improve the interaction of iron oxide and cerium oxide due to the increased oxygen vacancies, resulting in improved dispersion of iron oxide [30].

Based on these properties and the findings of previously mentioned studies at relatively mild conditions, this class of materials (Fe-Ce-Zr) may have application for high temperature (1100°C) iG-CLC as well. The present work focuses on measuring the oxygen transport capability of Fe-Ce-, Fe-Zr- and Fe-Ce-Zr-based oxygen carriers for multiple continuous redox cycles at 1100°C under iG-CLC conditions. High temperature iG-CLC is of particular interest to improve the performance and efficiency of the fuel reactor. The novel aspect of this study was to determine the reactivity and stability of Fe-Ce-Zr-based oxygen carriers at elevated temperatures. This temperature (1100°C) is higher than typically used in the fuel reactor (950°C) and required investigation with regard to the oxygen carrier performance and characteristics under reducing and oxidizing conditions. Carbon monoxide was generated as the reducing gas from in-situ CO₂-gasification of coal char at 1100°C. The formation of a Ce-Zr solid solution with Ce:Zr (3:1) was chosen to improve the oxygen carrier performance based on previously reported findings that produced optimal reactivity and redox stability. This study by Ma et al. (2018) focused on hydrogen generation from chemical-looping at 850°C. In this study, the authors found that Ce_{0.75}Zr_{0.25}O₂ had improved oxygen mobility and thermal stability compared to CeO₂ [27]. The Fe-Ce, Fe-Zr and Fe-Ce-Zr carriers were prepared, characterized, and tested in redox cycles in a drop tube fixed bed reactor (DT-FBR) to evaluate the oxygen transport capability. The optimal support (CeO₂-ZrO₂) composition was not investigated in this study. The major objective was to determine the performance of a Zr doped Fe₂O₃-CeO₂ oxygen carrier and compare this to iron oxide on a single support (Fe₂O₃-CeO₂ and Fe₂O₃-ZrO₂).

2. Experimental

2.1. Oxygen carrier materials

In this study, Fe-Ce, Fe-Zr and Fe-Ce-Zr oxygen carriers were prepared using a co-precipitation method. The amount of iron oxide used in each oxygen carrier was kept constant at 60wt% Fe₂O₃. The

desired amounts of precursor nitrates for Fe₂O₃, Fe(NO₃)₃·9H₂O (Sigma-Aldrich, ≥ 98% ACS) and supports, Ce(NO₃)₃·6H₂O (Aldrich, 99%) and/or ZrO(NO₃)₂·xH₂O (Aldrich, 99%) were dissolved in deionized water to produce a 3-molar solution. The resulting nitrate solutions were added together and heated to 70°C under constant mixing by a magnetic stirrer. A 25% ammonia solution was slowly added to increase the pH of the solution to 9. The precipitate solution was aged at room temperature for 12 hours and then filtered. The resulting solid precipitate was dried at 110°C for 24 hours under N₂, heated to 350°C for 2 hours under air to decompose the nitrates and then calcined at 850°C for 2 hours under air. The particles were ground using a mortar and pestle and sieved below 250 μm.

Three different oxygen carriers were made for this study: 60wt% Fe₂O₃ – 40wt% CeO₂ (Fe-Ce), 60wt% Fe₂O₃ – 40wt% ZrO₂ (Fe-Zr) and 60wt% Fe₂O₃ – 30wt% CeO₂ – 10wt% ZrO₂ (Fe-Ce-Zr). Elemental analysis of the three oxygen carriers was carried out by Inductively Coupled Plasma-Optical Emission Spectroscopy (ICP-OES) using a Perkin Elmer Optima 7300 DV system for Fe and Zr species and Inductively Coupled Plasma-Mass Spectrometry (ICP-MS) using a Nexion 350D system for cerium species. The calcined oxygen carriers were digested using microwave assisted aqua regia. The actual chemical compositions of the fresh oxygen carriers are given in Table 1. Additionally, CeO₂ (Ce) and 75wt% CeO₂ – 25wt% ZrO₂ (Ce-Zr) oxygen carriers were prepared by precipitation using the method mentioned above. These materials were synthesized to study the activity of the support materials without iron present.

Table 1. Elemental analysis of the Fe-Ce, Fe-Ce-Zr and Fe-Zr oxygen carriers by ICP-OES/MS.

	Fe ₂ O ₃ [wt%]	CeO ₂ [wt%]	ZrO ₂ [wt%]
Fe-Ce	64.0	36.0	-
Fe-Ce-Zr	61.7	31.0	7.3
Fe-Zr	64.6	-	35.4

2.2. Solid fuel preparation

The coal used to perform in-situ gasification chemical-looping combustion was a Powder River Basin (PRB) sub-bituminous coal. The samples that were used in this study were obtained from the U.S. Department of Energy's National Carbon Capture Center (NCCC). Coal char was generated by pyrolyzing the coal at 1000°C under flowing N₂ for 1 hour. The coal char was sieved to obtain a particle size of 250-500 µm. Proximate analysis results for the raw PRB coal and PRB char, obtained using ASTM D7582, are given in Table 2. After pyrolysis, the PRB char sample contained 87.74% fixed carbon and 12.26% ash on a dry basis.

Table 2. Proximate analysis of the PRB coal and PRB char generated at 1000°C.

	As Received [wt%]				Dry Basis [wt%]			
	Moisture	Volatile	Fixed Carbon	Ash	Moisture	Volatile	Fixed Carbon	Ash
PRB Coal	3.34	44.64	45.64	6.38	-	46.18	47.22	6.60
PRB Char	-	-	-	-	-	-	87.74	12.26

2.3. Oxygen carrier characterization

2.3.1. X-ray diffraction

The crystalline phase composition of the fresh and reacted (1100°C) oxygen carriers were determined by powder X-ray diffraction (XRD). The XRD analysis was done with a PANalytical X'Pert PRO multipurpose diffractometer that was equipped with a Cu anode. The anode of the X-ray diffractometer was operated at 45 kV and 40 mA with a divergent beam monochromator. Before XRD analysis, the

oxygen carrier samples were ground using a mortar and pestle to produce a powder. The crystalline phases that were identified by XRD were verified by comparing the results to the International Centre for Diffraction Data (ICDD) inorganic compound database.

2.3.2. Scanning electron microscopy

A scanning electron microscope (SEM) (FEI Company Quanta 450) was used to examine the oxygen carriers. The morphology and constituent (Fe, Ce, Zr) distributions were determined from SEM analysis. The oxygen carriers were set with conductive tape on aluminum planchets and examined with backscatter detection using a 10 mm working distance and a 20kV accelerating voltage. The sintering, agglomeration and location of the iron, cerium and zirconium species in the oxygen carriers were investigated.

2.3.3. Pore and surface area characterization

N₂ adsorption isotherms of the oxygen carriers were examined at 77K. This analysis was carried out to measure the pore volume and BET surface area of the fresh and reacted oxygen carriers using a Quantachrome Autosorb 1-C. Before beginning isotherm measurement, the oxygen carrier samples were degassed at 110°C overnight under vacuum. Multipoint BET analysis was done at relative pressures (P/P_0 = 0.007-0.04) and the total pore volume measurements were done at $P/P_0 \approx 0.99$. The surface area and pore volume of the micropores were determined using the t-method in the P/P_0 range of 0.15-0.45.

2.4. Drop tube fixed bed reactor (DT-FBR) set-up and procedure

The oxygen transport capability of the oxygen carriers was investigated using a drop tube fixed bed reactor (DT-FBR). The DT-FBR schematic is shown in Figure 1. The reactor tube was made of quartz with the dimensions 25mm OD x 22mm ID x 48in L. A 3-zone Lindberg/Blue M tube furnace was used to heat the reactor tube with a total heated length of 24 in. A K-type thermocouple, located beneath the porous support, was used to monitor the temperature at the bottom of the oxygen carrier bed. The feed gas flow rate was controlled and monitored by Alicat Scientific mass flow controller/meters. The oxygen carrier was loaded inside the reactor tube and sat on a porous bed support made from high-temperature (max 1426°C) ceramic fiber tape. Approximately 2.5 g of oxygen carrier was used for each test series. First, Ar gas was used to purge the reactor. The gas was vented through the purge valve at the top of the reactor. The coal char sample was loaded into the top of the reactor with the drop valve closed (Figure 1). During sample loading, the reactor was continuously purged with Ar. Afterwards, the reactor furnace was heated to the test temperature (1100°C) under Ar sweep gas.

After heating to 1100°C, the gas flow was switched to 20% CO₂ – 80% Ar. When the temperature and gas flow became steady, the drop valve was opened. The coal char fell into the reactor and on top of the oxygen carrier bed. Two different amounts of coal char were used in this study. The lower amount of coal char (0.06 g char) is related to the stoichiometric amount of carbon needed to react all the Fe₂O₃ to Fe₃O₄. The higher amount of coal char (0.12 g char) represents a condition where the carbon fuel is in excess. Fresh char was loaded into the reactor for each cycle and dropped onto the oxygen carrier bed. In-situ CO₂ gasification occurred which generated the reaction gas CO. After reaction, the gas flow rate was switched to ~22% O₂ – balance Ar to re-oxidize the oxygen carrier. This entire process was repeated for the desired number of cycles. The concentrations of CO, CO₂, O₂ and Ar leaving the reactor were measured with a quadrupole mass spectrometer (QMS) at approximately 0.8 second intervals. The QMS used in this study was a Pfeiffer OmniStar GSD 301. A summary of the experimental conditions used for reduction and oxidation cycles are given in Table 3.

Table 3. Experimental conditions for reduction and oxidation cycles.

	Reduction	Oxidation
Reaction Time	10 min	10 min
Gas	CO (from char CO ₂ gasification 20 mol% CO ₂ – 80 mol% Ar)	22 mol% O ₂ – 78 mol% Ar
Flow Rate	500 sccm	500 sccm
Temp.	1100°C	1100°C

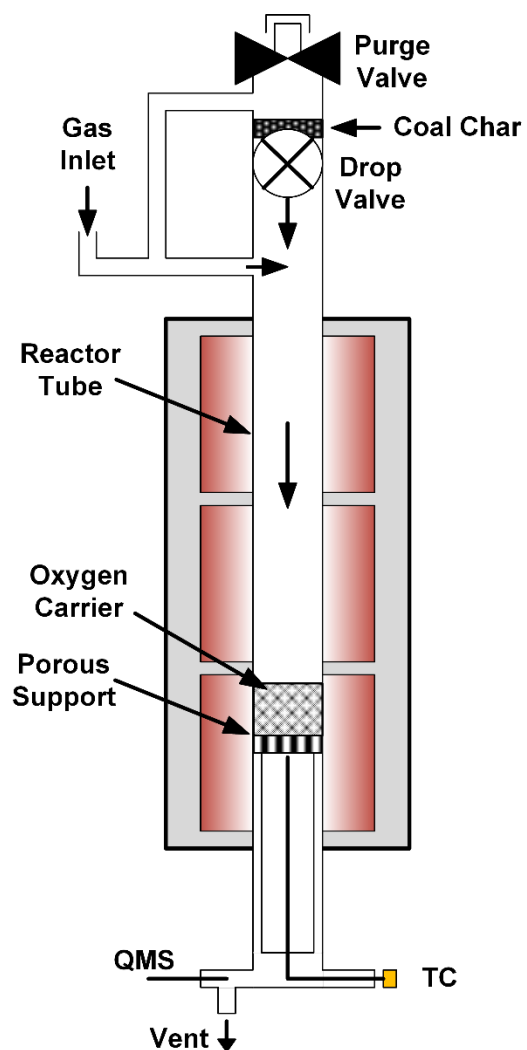


Figure 1. Drop tube fixed bed reactor (DT-FBR) schematic.

2.5. Evaluation of oxygen transport capability of the oxygen carriers

The effectiveness of the oxygen carrier was evaluated based on how much oxygen it was able to provide for reaction with the fuel during each cycle. The material balance equations for the reactions involving the oxygen carriers were derived for this reactor in Equations 1-6. The total volumetric flow rate of the gases leaving the reactor was calculated from:

$$F_{Total} = \frac{F_{Ar}}{1 - X_{CO} - X_{CO_2}} \quad (1)$$

where F_{Total} and F_{Ar} are the volumetric flow rates leaving the reactor at standard temperature and pressure (STP) of all gases and Ar respectively. X_{CO} and X_{CO_2} are the measured concentrations (mole fractions) of CO and CO₂, respectively. The volumetric flow rate of CO leaving the reactor (F_{CO}) is:

$$F_{CO} = F_{Total} X_{CO} \quad (2)$$

The flow rate for CO₂ leaving the reactor (F_{CO_2}) is calculated in a similar manner. The volumetric flow rates (STP) are simply converted to molar flow rates n_{CO} and n_{CO_2} . The total number of moles of CO leaving the reactor is calculated from:

$$N_{CO} = \int_0^t n_{CO} dt \quad (3)$$

The moles of CO₂ leaving the reactor (N_{CO_2}) is also calculated using this method.

The oxygen transport capability X_O of the oxygen carriers is the number of moles of oxygen transferred from the solid phase (oxygen carrier) to the gas phase and defined by:

$$X_O = [N_{O,CO_2 out} + N_{O,CO out}] - N_{O,CO_2 in} \quad (4)$$

$$N_{O,CO} = N_{CO} \quad (5)$$

$$N_{O,CO_2} = 2 N_{CO_2} \quad (6)$$

The first term in Equation 4 is the moles of oxygen leaving the reactor in the gas phase from CO and CO₂. The parameter $N_{O,CO_2 in}$ is the moles of oxygen in the inlet stream from CO₂ used for in-situ gasification of the coal char. In this study, the concentration of CO, CO₂ and Ar were determined by a quadrupole mass spectrometer and the Ar flow rate was measured by a mass flow controller.

3. Results and discussion

3.1. Oxygen carrier characterization

The XRD patterns for the Ce, Ce-Zr, Fe-Ce, Fe-Ce-Zr and Fe-Zr oxygen carriers are shown in Figure 2. The Ce oxygen carrier was initially CeO₂ and remained as CeO₂ after the 10th reduction cycle. The CeO₂ became more crystallized after reaction but remained cerium (IV) oxide indicating that oxygen transport was due to the creation of oxygen vacancies. Before reaction, the Ce-Zr oxygen carrier was a mixture of CeO₂ and tetragonal ZrO₂. After redox cycling the oxygen carrier, a CeO₂-ZrO₂ solid solution formed where Zr was substituted into the CeO₂ fluorite structure.

The fresh Fe-Ce oxygen carrier contained Fe₂O₃ and CeO₂. After 10 redox cycles, cerium orthoferrite (CeFeO₃) was observed with Fe₃O₄ and CeO₂. This material formed from the reaction of iron oxide with ceria. CeFeO₃ was reported to be made by the solid state reactions: $3CeO_2 + Fe_2O_3 + Fe \rightarrow 3CeFeO_3$ or $CeO_2 + FeO \rightarrow CeFeO_3$ [31, 32]. The CeFeO₃ formed as a result of Fe₂O₃ reduction. The addition of iron to the Ce-Zr support in the fresh Fe-Ce-Zr oxygen carrier resulted in CeO₂-ZrO₂ solid solutions and Fe₂O₃. The CeO₂-ZrO₂ material was identified to be Ce_{0.75}Zr_{0.25}O₂, which was the target composition during synthesis. After 10 redox cycles, CeFeO₃ formed again from the reaction of iron oxide and ceria. Fe₃O₄

and $\text{Ce}_{0.75}\text{Zr}_{0.25}\text{O}_2$ were also observed. The amount of CeFeO_3 that formed was significantly less than with the Fe-Ce oxygen carrier. This indicated that the addition of Zr into the CeO_2 fluorite structure impeded the reaction of iron oxide and ceria. The Fe-Zr oxygen carrier initially contained Fe_2O_3 and ZrO_2 (monoclinic and tetragonal). After 10 redox cycles, Fe_3O_4 was formed with some tetragonal ZrO_2 becoming monoclinic ZrO_2 .

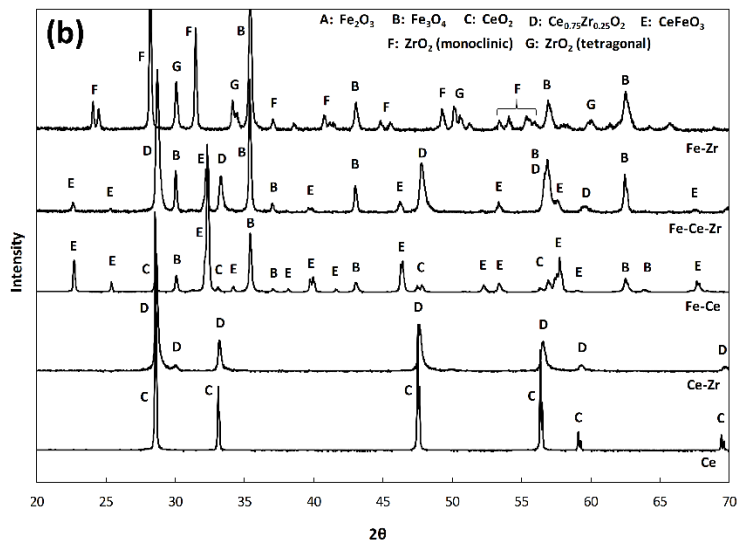
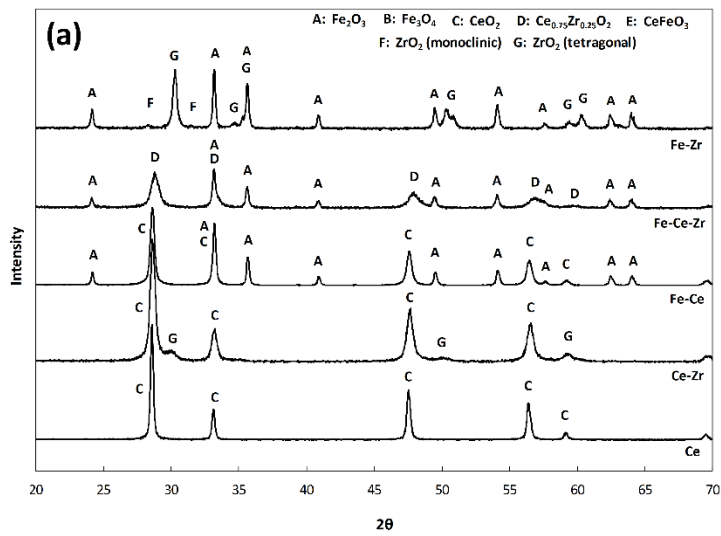


Figure 2. XRD patterns of (a) fresh and (b) after reduction (10 cycles) for the Ce, Ce-Zr, Fe-Ce, Fe-Ce-Zr and Fe-Zr oxygen carriers.

The oxygen carriers were analyzed by scanning electron microscopy (SEM) with backscatter detection. Figure 3 shows the SEM images of the Fe-Ce and Fe-Ce-Zr oxygen carriers before the test and after the tenth reduction step at 1100°C. The SEM analysis revealed separation of the iron from cerium and zirconium species. Before reaction, the Fe-Ce (a) and Fe-Ce-Zr (b) oxygen carriers had uniformly distributed Fe-, Ce-, and Zr-species. After reaction, species separation was observed in the oxygen carriers. Due to the size of these features, more detailed elemental analysis from SEM was not able to be obtained. Backscatter detection from SEM showed features with differing atomic number. This was most evident in the Fe-Ce sample (c) where the lighter regions are Ce-rich, and the darker regions are Fe-rich. When zirconium was added to the oxygen carrier, less species separation occurred. The Fe-Ce-Zr sample (d) showed smaller species separated regions after 10 redox cycles at 1100°C. The lighter shaded clusters in the SEM image are areas where Ce and/or Zr has separated from Fe-based species. The addition of Zr to the oxygen carrier was shown to help stabilize the solid solution of cerium and iron.

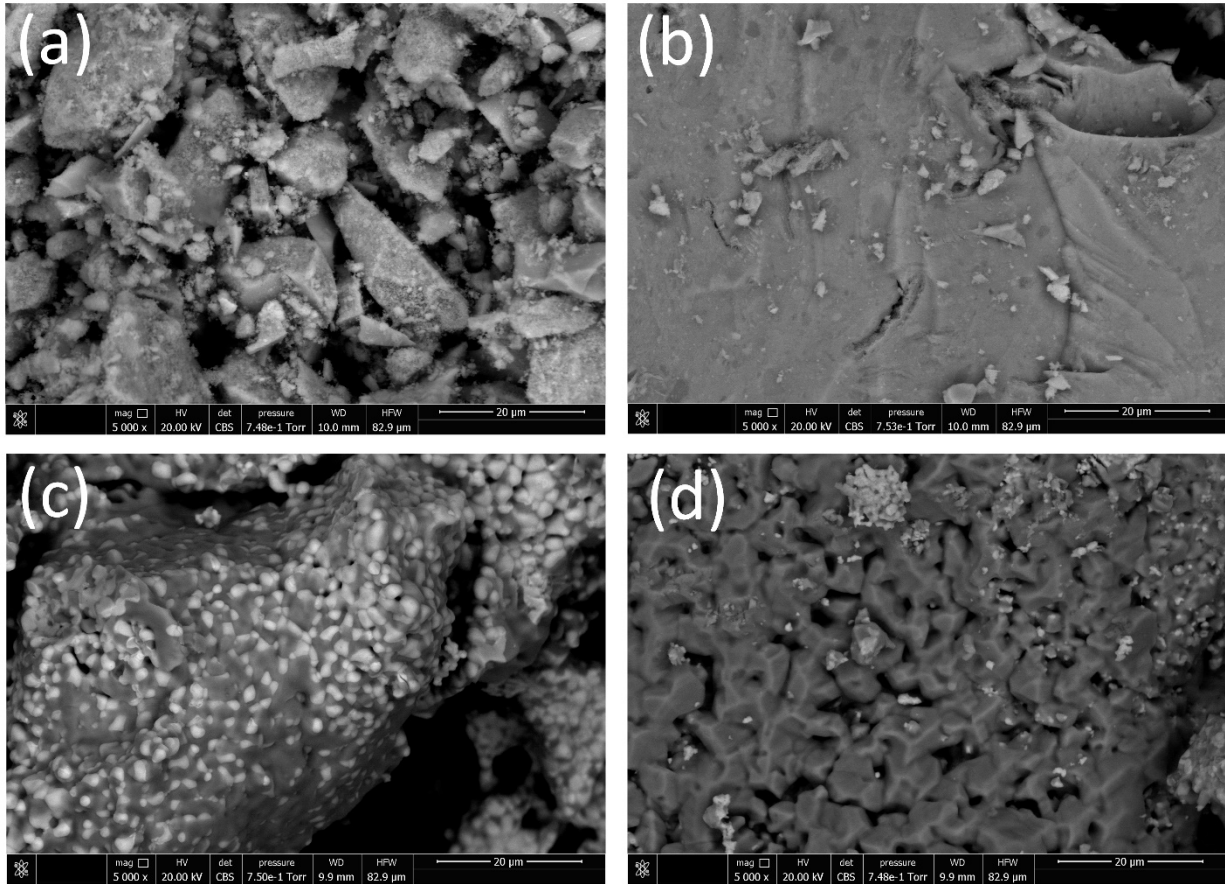


Figure 3. SEM images of the raw unreacted oxygen carriers: (a) Fe-Ce and (b) Fe-Ce-Zr, and after 10 redox cycles with excess char at 1100°C: (c) Fe-Ce and (d) Fe-Ce-Zr.

3.2. Oxygen transport capability after multiple redox cycles

The reactivity and stability of the oxygen carriers were investigated at 1100°C under iG-CLC conditions. The reactive gas (CO) was generated from in-situ CO₂-gasification of coal char. The normalized oxygen transport capability of the Fe-Ce oxygen carrier during the reduction step of cycle # 5 is shown in Figure 4. The amount of oxygen transferred from the oxygen carrier to the product gas was normalized based on the iron content of the material. Two different amounts of coal char were used in this study. The lower amount of coal char (0.06 g char) is related to the stoichiometric amount of carbon needed to

react all the Fe_2O_3 to Fe_3O_4 . The higher amount of coal char (0.12 g char) represents a condition where the carbon fuel is in excess. With higher amounts of coal char, the oxygen transport capability increases, allowing Fe_2O_3 to be further reduced to FeO . At longer reaction times in the excess char test series, the oxygen transport capability reaches a maximum and then goes down due to the soft oxidation of FeO to Fe_3O_4 from CO_2 present in the gas feed. This is observed to a lesser extent in the stoichiometric char test series. For the multi-cycle comparison, the peak maximum oxygen transport capability was evaluated before the soft oxidation (around 2 – 3 minutes).

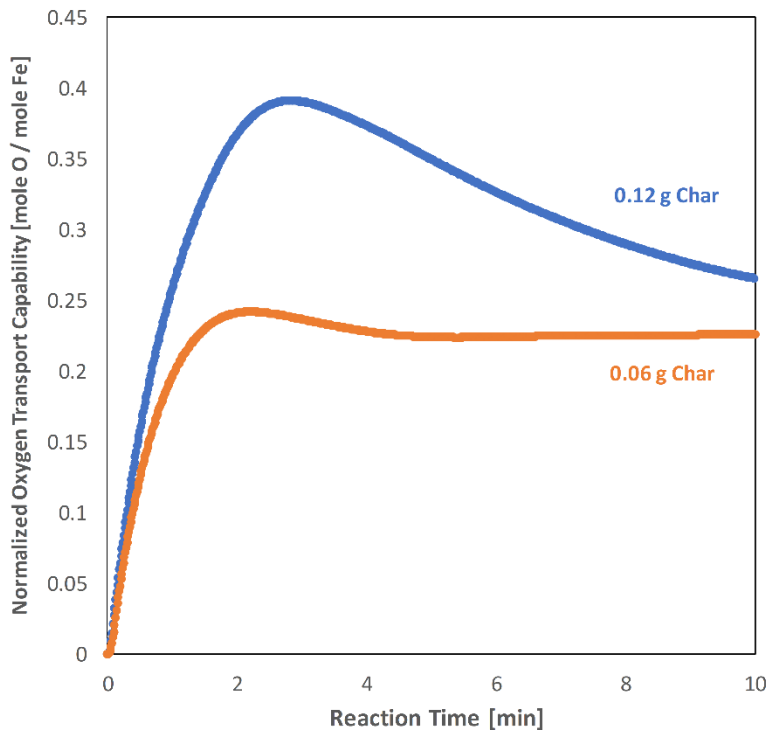


Figure 4. Normalized oxygen transport capability over time of the Fe-Ce oxygen carrier during cycle # 5 with two different amounts of coal char.

The Ce and Ce-Zr support materials were also tested at 1100°C under iG-CLC conditions. These materials were evaluated using the excess amount of coal char. The oxygen transport capabilities of these support materials were evaluated using the same method as the Fe-Ce, Fe-Ce-Zr and Fe-Zr oxygen carriers. The amount of oxygen transferred from the active support to the product gas was normalized based on the Ce or Ce + Zr content of the material. For the Ce support, the normalized oxygen transport capability was 0.081 mole O / mole Ce. The Ce-Zr support had 0.121 mole O / mole Ce+Zr. These tests showed that oxygen transport from the support occurred due to the creation of oxygen vacancies. Additionally, the doping of CeO₂ with Zr⁴⁺ made it easier for oxygen defects to form, which improved the oxygen mobility.

The maximum oxygen transport capability for the Fe-Ce, Fe-Ce-Zr and Fe-Zr oxygen carriers over 10 redox cycles is shown in Figure 5. The theoretical oxygen transport capability (dashed lines) for Fe₂O₃ → Fe₃O₄ and Fe₂O₃ → Fe₃O₄ → FeO are shown in Figure 5 for reference. All three oxygen carriers showed good stability over 10 redox cycles at 1100°C. In the stoichiometric coal char test series, the oxygen transport capability corresponded to the reduction of Fe₂O₃ to Fe₃O₄. This is evident from the Fe-Zr oxygen carrier which had no additional oxygen transport from the support or interaction between the iron and zirconia. The Fe-Ce and Fe-Ce-Zr oxygen carriers had oxygen transport capabilities higher than Fe-Zr for all 10 redox cycles. Additional oxygen was provided from the Ce and Ce-Zr supports. The Fe-Ce oxygen carrier provided more oxygen for combustion than the Fe-Ce-Zr for most of the redox cycles. As the number of cycles increased, the oxygen transport capability of the Fe-Ce and Fe-Ce-Zr oxygen carriers approached the same value.

The Fe-Ce oxygen carrier showed a higher oxygen transport capability than the Fe-Ce-Zr oxygen carrier. This is the opposite trend from the test with the Ce and Ce-Zr supports which showed that Ce-Zr had a higher oxygen transport capability due to the creation of more oxygen vacancies. The reason for this change is due to the formation of cerium orthoferrite (CeFeO₃). CeFeO₃ is a perovskite material which can provide even more oxygen for combustion through the creation of additional oxygen vacancies.

CeFeO₃ is highly stable under reducing conditions but unstable in an oxidizing environment [32]. The CeO₂-ZrO₂ solid solution impeded the formation of CeFeO₃ based on XRD analysis. The oxygen transport capability of the Fe-Ce-Zr oxygen carrier increased during the later cycles and approached the value for the Fe-Ce oxygen carrier (Figure 5). This may be attributed to the eventual formation of CeFeO₃ in the Fe-Ce-Zr oxygen carrier. This separation was observed by XRD analysis in the excess char samples where CeFeO₃ was identified after 10 redox cycles.

In the excess coal char test series, the oxygen transport capabilities of the Fe-Ce and Fe-Ce-Zr oxygen carriers were even higher than the Fe-Zr oxygen carrier. As Fe₂O₃ further reduced from Fe₃O₄ to FeO, more CeFeO₃ formed in the oxygen carrier sample. The increased amount of CeFeO₃ in the Fe-Ce and Fe-Ce-Zr samples resulted in a greater oxygen transport capability compared to the Fe-Zr sample. As the number of redox cycles increased, the oxygen transport capabilities of the Fe-Ce and Fe-Ce-Zr approached the same value due to more CeFeO₃ forming in the Fe-Ce-Zr oxygen carrier upon subsequent reduction reactions. The formation of CeFeO₃ was observed by XRD analysis. CeFeO₃ in the Fe-Ce oxygen carrier decreases upon subsequent redox cycles due to poor stability under oxidizing conditions [32], whereas CeFeO₃ in the Fe-Ce-Zr oxygen carrier increases as iron oxide is repeatedly reduced and oxidized in the presence of CeO₂.

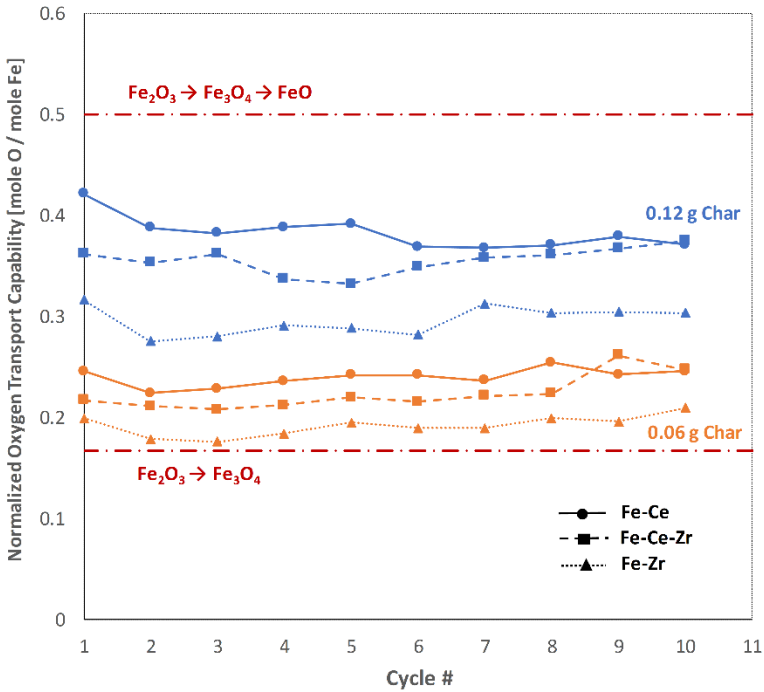


Figure 5. Normalized oxygen transport capability of the Fe-Ce, Fe-Ce-Zr and Fe-Zr oxygen carriers with two different amounts of coal char.

The initial rate of oxygen transport was evaluated for the Fe-Ce, Fe-Ce-Zr and Fe-Zr oxygen carriers. No significant trend was observed for the stoichiometric char test series. However, the initial oxygen transport rate in the excess char test series decreased at higher redox cycles for the Fe-Ce and Fe-Ce-Zr oxygen carriers (Figure 6). A smaller change was observed for the Fe-Zr oxygen carrier. The decrease in initial oxygen transport rate may be attributed to two factors: irreversible phase change during reduction forming CeFeO_3 and loss of available surface area due to sintering and agglomeration. The oxygen transport mechanism of perovskite-type CeFeO_3 involves the formation of oxygen vacancies and this differs from the redox states of iron oxide. Multipoint BET measurements showed that the Fe-Ce surface area decreased from $8.483 \text{ m}^2/\text{g}$ to $0.041 \text{ m}^2/\text{g}$ for cycle #1 to cycle #10. Similarly, the Fe-Ce-Zr oxygen carrier showed a decrease in surface area from $8.262 \text{ m}^2/\text{g}$ to $0.690 \text{ m}^2/\text{g}$ after ten redox cycles.

The reactions at 1100°C causes a loss of surface area in all of the oxygen carrier samples. As a result, the differences in oxygen transport capability and oxygen transport rate between the Fe-Ce and Fe-Ce-Zr oxygen carriers likely depends on the species that change (CeFeO_3 and $\text{Ce}_{0.75}\text{Zr}_{0.25}\text{O}_2$) during subsequent redox reactions. This loss of reactivity was observed in the excess char test series due to the greater degree of iron oxide reduction. As the number of redox cycles increased, the reactivity of the Fe-Ce-Zr oxygen carrier performed better than the Fe-Ce oxygen carrier due to the improved redox properties of the CeO_2 - ZrO_2 solid solution. CeO_2 - ZrO_2 has higher oxygen transport capability than CeO_2 because doping CeO_2 with Zr^{4+} reduces strain within the metal oxide and makes it easier for oxygen defects to form. This change improves the oxygen mobility of CeO_2 - ZrO_2 compared to CeO_2 .

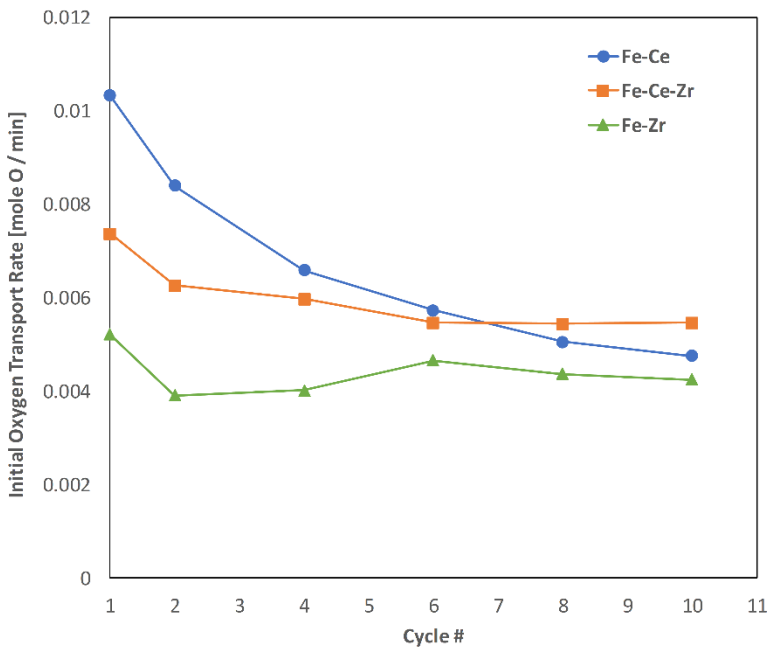


Figure 6. Initial oxygen transport rate of the Fe-Ce, Fe-Ce-Zr and Fe-Zr oxygen carriers using excess coal char.

4. Conclusion

The Fe-Ce, Fe-Zr and Fe-Ce-Zr oxygen carriers prepared by co-precipitation were investigated in a drop tube fixed bed reactor with iG-CLC at 1100°C. The CeO₂-ZrO₂ material was identified to be Ce_{0.75}Zr_{0.25}O₂, which was the target composition during synthesis. The oxygen transport capabilities of the oxygen carriers were investigated over 10 redox cycles. In the Fe-Ce-Zr oxygen carrier, a CeO₂-ZrO₂ solid solution formed where Zr was substituted into the CeO₂ fluorite structure. After multiple redox cycles, cerium orthoferrite (CeFeO₃) was observed in the Fe-Ce and Fe-Ce-Zr oxygen carriers. The addition of Zr into the CeO₂ fluorite structure impeded the reaction of iron oxide and ceria. Additionally, the doping of CeO₂ with Zr⁴⁺ made it easier for oxygen defects to form which improved the oxygen mobility. The Fe-Ce oxygen carrier showed a higher oxygen transport capability than the Fe-Ce-Zr oxygen carrier due to the formation of more cerium orthoferrite (CeFeO₃) which is a perovskite-type material and can provide even more oxygen transport. The initial oxygen transport rate in the excess char test series decreased with redox cycles for the Fe-Ce and Fe-Ce-Zr oxygen carriers due to formation of more CeFeO₃ and loss of available surface area resulting from sintering and agglomeration. Additionally, separation of cerium and/or zirconium from iron species was observed after redox cycles at 1100°C. This may also account for the sintering and the observed loss of oxygen carrier activity. Overall, these oxygen carriers are good candidates for high temperature operation because they showed relatively stable oxygen transport over multiple redox cycles at 1100°C. The addition of Zr to the oxygen carrier helped stabilize the solid solution of cerium and iron, which may provide additional stability during high temperature redox cycles.

Author Information

Corresponding Author

E-mail: nicholas.means@netl.doe.gov

Notes

The authors declare no competing financial interest.

Acknowledgment

This work was performed in support of the US Department of Energy's Fossil Energy Crosscutting Technology Research Program. The Research was executed through the NETL Research and Innovation Center's Advanced Combustion – CLC Field Work Proposal. Research performed by Leidos Research Support Team staff was conducted under the RSS contract 89243318CFE000003.

Disclaimer

This work was funded by the Department of Energy, National Energy Technology Laboratory, an agency of the United States Government, through a support contract with Leidos Research Support Team (LRST). Neither the United States Government nor any agency thereof, nor any of their employees, nor LRST, nor any of their employees, makes any warranty, expressed or implied, or assumes any legal liability or responsibility for the accuracy, completeness, or usefulness of any information, apparatus, product, or process disclosed, or represents that its use would not infringe privately owned rights. Reference herein to any specific commercial product, process, or service by trade name, trademark, manufacturer, or otherwise, does not necessarily constitute or imply its endorsement, recommendation, or favoring by the United States Government or any agency thereof. The views and opinions of authors expressed herein do not necessarily state or reflect those of the United States Government or any agency thereof.

References

1. Thomas, D.J., *Finding a future for clean coal and CO₂ storage technology*. Fuel, 2017. **195**: p. 314-315.

2. Lewis, W.K., N. Gilliland, and E.R. Gilliland, *Production of Pure Carbon Dioxide*. 1954: USA.
3. Adanez, J., et al., *Progress in Chemical-Looping Combustion and Reforming Technologies*. Progress in Energy and Combustion Science, 2012. **38**: p. 215-282.
4. Jerndal, E., T. Mattisson, and A. Lyngfelt, *Thermal Analysis of Chemical-Looping Combustion*. Chemical Engineering Research and Design, 2006. **84**: p. 795-806.
5. Adanez, J., et al., *Selection of Oxygen Carriers for Chemical-Looping Combustion*. Energy & Fuels, 2004. **18**: p. 371-377.
6. Abad, A., et al., *Mapping of the range of operational conditions for Cu-, Fe-, and Ni-based oxygen carriers in chemical-looping combustion*. Chemical Engineering Science, 2007. **62**: p. 533-549.
7. Mattisson, T., M. Johansson, and A. Lyngfelt, *Multicycle Reduction and Oxidation of Different Types of Iron Oxide Particles - Application to Chemical-Looping Combustion*. Energy & Fuels, 2004. **18**: p. 628-637.
8. Johansson, M., T. Mattisson, and A. Lyngfelt, *Investigation of Fe₂O₃ with MgAl₂O₄ for Chemical-Looping Combustion*. Industrial & Engineering Chemistry Research, 2004. **43**: p. 6978-6987.
9. Cho, P., T. Mattisson, and A. Lyngfelt, *Defluidization Conditions for a Fluidized Bed of Iron Oxide-, Nickel Oxide-, and Manganese Oxide-Containing Oxygen Carriers for Chemical-Looping Combustion*. Industrial & Engineering Chemistry Research, 2006. **45**: p. 968-977.
10. Jin, H., T. Okamoto, and M. Ishida, *Development of a Novel Chemical-Looping Combustion: Synthesis of a Solid Looping Material of NiO/NiAl₂O₄*. Industrial & Engineering Chemistry Research, 1999. **38**: p. 126-132.
11. Ishida, M., H. Jin, and T. Okamoto, *Kinetic Behavior of Solid Particle in Chemical-Looping Combustion: Suppressing Carbon Deposition in Reduction*. Energy & Fuels, 1998. **12**: p. 223-229.
12. Jin, H., T. Okamoto, and M. Ishida, *Development of a Novel Chemical-Looping Combustion: Synthesis of a Looping Material with a Double Metal Oxide of CoO-NiO*. Energy & Fuels, 1998. **12**: p. 1272-1277.
13. Ishida, M. and H. Jin, *A Novel Combustor Based on Chemical-Looping Reactions and Its Reaction Kinetics*. Journal of Chemical Engineering of Japan, 1994. **27**(3): p. 296-301.
14. Wright, J.K. and R.J. Tyler, *Pore structure of sintered and metallized iron oxide compacts*. Powder Technology, 1979. **24**(1): p. 49-55.
15. Zafar, Q., T. Mattisson, and B. Gevert, *Integrated Hydrogen and Power Production with CO₂ Capture Using Chemical-Looping Reforming - Redox Reactivity of Particles of CuO, Mn₂O₃, NiO, and Fe₂O₃ Using SiO₂ as a Support*. Industrial & Engineering Chemistry Research, 2005. **44**: p. 3485-3496.
16. Kaspar, J., P. Fornasiero, and N. Hickey, *Automotive catalytic converters: current status and some perspectives*. Catalysis Today, 2003. **77**: p. 419-449.
17. Bhattacharyya, A., A., et al., *Catalytic SO_x Abatement: The Role of Magnesium Aluminate Spinel in the Removal of SO_x from Fluid Catalytic Cracking (FCC) Flue Gas*. Industrial & Engineering Chemistry Research, 1988. **27**: p. 1356-1360.
18. Liu, W. and M. Flytzani-Stephanopoulos, *Total Oxidation of Carbon Monoxide and Methane over Transition Metal-Fluorite Oxide Composite Catalysts*. Journal of Catalysis, 1995. **153**: p. 304-316.
19. Pengpanich, S., et al., *Catalytic oxidation of methane over CeO₂-ZrO₂ mixed oxide solid solution catalysts prepared via urea hydrolysis*. Applied Catalysis A: General, 2002. **234**: p. 221-233.
20. Gorte, R.J. and S. Zhao, *Studies of the water-gas-shift reaction with ceria-supported precious metals*. Catalysis Today, 2005. **104**: p. 18-24.
21. Trovarelli, A., *Catalytic Properties of Ceria and CeO₂-Containing Materials*. Catalysis Reviews, 1996. **38**(4): p. 439-520.
22. Huang, H.B., et al., *Chemical looping combustion of biomass-derived syngas using ceria-supported oxygen carriers*. Bioresource Technology, 2013. **140**: p. 385-391.

23. Guerrero-Caballero, J., et al., *Ni, Co, Fe supported on Ceria and Zr doped Ceria as oxygen carriers for chemical looping dry reforming of methane*. Catalysis Today, 2019. **In Press**.
24. Hedayati, A., et al., *Evaluation of Novel Ceria-Supported Metal Oxides As Oxygen Carriers for Chemical-Looping Combustion*. Industrial & Engineering Chemistry Research, 2012. **51**: p. 12796-12806.
25. Galinsky, N.L., et al., *Effect of support on the redox stability of iron oxide for chemical looping conversion of methane*. Applied Catalysis B: Environmental, 2015. **164**: p. 371-379.
26. Ma, S., et al., *Effects of CeO₂, ZrO₂, and Al₂O₃ Supports on Iron Oxygen Carrier for Chemical Looping Hydrogen Generation*. Energy & Fuels, 2017. **31**: p. 8001-8013.
27. Ma, S., et al., *Effects of Zr doping on Fe₂O₃/CeO₂ oxygen carrier in chemical looping hydrogen generation*. Chemical Engineering Journal, 2018. **346**: p. 712-725.
28. Damyanova, S., et al., *Study of the surface and redox properties of ceria-zirconia oxides*. Applied Catalysis A: General, 2008. **337**: p. 86-96.
29. Oliveira, C.F., et al., *Effects of preparation and structure of cerium-zirconium mixed oxides on diesel soot catalytic combustion*. Applied Catalysis A: General, 2012. **413-414**: p. 292-300.
30. Li, K., et al., *Partial oxidation of methane to syngas with air by lattice oxygen transfer over ZrO₂-modified Ce-Fe mixed oxides*. Chemical Engineering Journal, 2011. **173**: p. 574-582.
31. Robbins, M., et al., *Preparation and properties of polycrystalline cerium orthoferrite (CeFeO₃)*. Journal of Physics and Chemistry of Solids, 1969. **30**: p. 1823-1825.
32. Li, K., et al., *Modification of CeO₂ on the redox property of Fe₂O₃*. Materials Letters, 2013. **93**: p. 129-132.